Chemical Science

EDGE ARTICLE

View Article Online
View Journal | View Issue

Cite this: *Chem. Sci.*, 2016, **7**, 3667

On the origin of high ionic conductivity in Na-doped $SrSiO_3$†

Po-Hsiu Chien,[a] Youngseok Jee,[b] Chen Huang,[c] Riza Dervişoğlu,[d] Ivan Hung,[e] Zhehong Gan,[e] Kevin Huang[b] and Yan-Yan Hu*[ae]

Received 9th November 2015
Accepted 17th February 2016

DOI: 10.1039/c5sc04270d

www.rsc.org/chemicalscience

Understanding the local structure and ion dynamics is at the heart of ion conductor research. This paper reports on high-resolution solid-state ^{29}Si, ^{23}Na, and ^{17}O NMR investigation of the structure, chemical composition, and ion dynamics of a newly discovered fast ion conductor, Na-doped $SrSiO_3$, which exhibited a much higher ionic conductivity than most of current oxide ion conductors. Quantitative analyses reveal that with a small dose (<10 mol%) of Na, the doped Na integrates into the $SrSiO_3$ structure to form $Na_xSr_{1-x}SiO_{3-0.5x}$, and with >10 mol% Na doping, phase separation occurs, leading to the formation of an amorphous phase β-$Na_2Si_2O_5$ and a crystalline Sr-rich phase. Variable-temperature ^{23}Na and ^{17}O magic-angle-spinning NMR up to 618 °C have shown significant changes in Na ion dynamics at high temperatures but little oxide ion motion, suggesting that Na ions are responsible for the observed high ionic conductivity. In addition, β-$Na_2Si_2O_5$ starts to crystallize at temperatures higher than 480 °C with prolonged heating, resulting in reduction in Na^+ motion, and thus degradation of ionic conductivity. This study has contributed critical evidence to the understanding of ionic conduction in Na-doped $SrSiO_3$ and demonstrated that multinuclear high-resolution and high-temperature solid-state NMR is a uniquely useful tool for investigating ion conductors at their operating conditions.

Introduction

A new family of complex oxides with an apparent composition $Na_xSr_{1-x}SiO_{3-0.5x}$ (SNS hereinafter) has recently been reported as a potential solid-state oxide-ion electrolyte.[1,2] The ionic conductivity of SNS with $x = 0.45$ reaches 0.01 S cm^{-1} at 500 °C, the highest among all known chemically stable oxide-ion conductors. Due to the significance of an ion conductor with high conductivity in electrochemical devices such as fuel cells, batteries, separation membranes, and sensors, SNS immediately garnered much attention and invited a number of follow-up studies after the first publication. The origin and mechanism of the ionic conduction observed in SNS were the two most discussed and debated topics. The original work by Singh *et al.*[1] and Martinez-Coronado *et al.*[3] with high-temperature neutron diffraction studies suggested that oxide-ion conduction *via* oxygen vacancies created by Na-doping was responsible for the observed high conductivity. This hypothesis appeared to be supported by Xu *et al.* with ^{29}Si NMR studies on a similar system, *i.e.*, K-doped $SrSiO_3$.[3,4] On the other hand, Bayliss *et al.*[5] argued that SNS was virtually a mixture of a $SrSiO_3$ phase and a glassy phase with a degrading conductivity. Their DFT calculations concluded that creation of oxygen vacancies by Na-doping was energetically prohibitive.[5] The subsequent ToF-SIMS measurement revealed a very low oxygen diffusion coefficient,[5] suggesting that oxide-ion conduction in SNS was indeed negligible and other ions should be responsible for the conduction. Several very recent studies further supported Bayliss's arguments on the two-phase composition and identified the glassy phase as $Na_2Si_2O_5$ by ^{29}Si NMR.[6,7] Jee *et al.*[8] also proved that the high conductivity of SNS was originated from the glassy $Na_2Si_2O_5$ and the degradation of conductivity stemmed from the crystallization of the glassy $Na_2Si_2O_5$ by high-temperature XRD and thermal analysis.

While these early studies suggested that the glassy $Na_2Si_2O_5$ phase was responsible for the high conductivity, the identity of ions responsible for high ionic conduction in the glassy $Na_2Si_2O_5$ remains ambiguous. A very recent *ab initio* molecular dynamics simulations on the glassy $Na_2Si_2O_5$ phase suggested that Na ions possess higher mobility in the structure compared with oxide ions[9] and variable-temperature ^{23}Na NMR spectroscopy and T_1 relaxation time measurements demonstrated

[a]*Department of Chemistry and Biochemistry, Florida State University, Tallahassee, FL 32306, USA. E-mail: hu@chem.fsu.edu*

[b]*Department of Mechanical Engineering, University of South Carolina, Columbia, SC 29208, USA*

[c]*Department of Scientific Computing, Florida State University, Tallahassee, FL 32306, USA*

[d]*Institute for Molecules and Materials, Radboud University, Nijmegen, AJ 6525, Netherland*

[e]*Centre of Interdisciplinary Magnetic Resonance, National High Magnetic Field Laboratory, 1800 East Paul Dirac Drive, Tallahassee, FL 32310, USA*

† Electronic supplementary information (ESI) available: NMR spectra, deconvolution results, and DFT calculations. See DOI: 10.1039/c5sc04270d

Na-ion mobility from room temperature to 350 °C.[10] However, experimental evidence is necessary to explain the temperature-dependence of Na^+ conduction at the operating temperature of SNS and experimental tools are needed to directly probe the O^{2-} dynamics. It is extremely challenging to use conventional diffraction methods to obtain information on local structural defects and to be specific enough in determining chemical phases with elemental mapping methods.[11]

Solid-state NMR possesses unique capabilities of probing the local defect structure and ion dynamics in ion conductors.[12–19] ^{29}Si NMR has been previously demonstrated to help understand the silicate network in SNS and to be useful for preliminary identification of chemical phases.[4–7] However, the information obtained was largely relevant to the local structural environment of SiO_x, not Na^+ or O^{2-} of interest. In fact, ^{23}Na and ^{17}O NMR have been employed in limited studies in the area of energy materials research due to the great challenges in detection sensitivity and spectral resolution. ^{23}Na and ^{17}O NMR often require high magnetic field and fast sample spinning in order to achieve high spectral resolution for reliable quantification. In particular, ^{17}O NMR is a very powerful tool for studying O^{2-} local structure and dynamics. However, due to the low natural abundance and low gyromagnetic ratio of the ^{17}O isotope, ^{17}O NMR is highly challenging in data acquisition and its invaluable potential in addressing critical questions in the area of oxide ion conductors has not been fully exploited.

In this paper, we report the employment of high-resolution ^{23}Na, ^{17}O and ^{29}Si NMR to track changes in the local structural environments of Na^+ and O^{2-} and the silicate framework of SNS. Careful chemical phase identification and quantification based on high-resolution NMR spectra were performed to understand the evolution in chemical phase composition when the Na content was gradually increased in SNS. Variable-temperature (VT) ^{23}Na and ^{17}O Magic-Angle-Spinning (MAS) NMR experiments were also carried out from room temperature to 618 °C on the sample (SNS45, *i.e.*, $x = 0.45$ in the apparent composition $Na_xSr_{1-x}SiO_{3-0.5x}$) with the highest ionic conductivity to probe the Na^+ and O^{2-} dynamics. This comprehensive study on chemical composition, local structure, and ion dynamics provides strong and direct experimental evidence for resolving the current debate on the origin of high ionic conductivity observed in SNS. The study is essential in that it helps assess the prospects of SNS as a potential O^{2-} or Na^+ conductor and provides guidelines for designing alternative ion conductors. It also demonstrates to the energy materials research community at large that advanced solid-state NMR is a versatile tool to address the most relevant questions in the field of ion conductors.

Results

SiO_x structural frame

^{29}Si NMR spectra of SNS0, SNS10, SNS20, SNS30, SNS40, SNS45, SNS70, and β-$Na_2Si_2O_5$ were acquired to investigate the effects of Na doping on the SiO_x structural frame and chemical phase composition. As shown in Fig. 1, the ^{29}Si spectrum of SNS0 (without Na doping) shows a single sharp resonance at

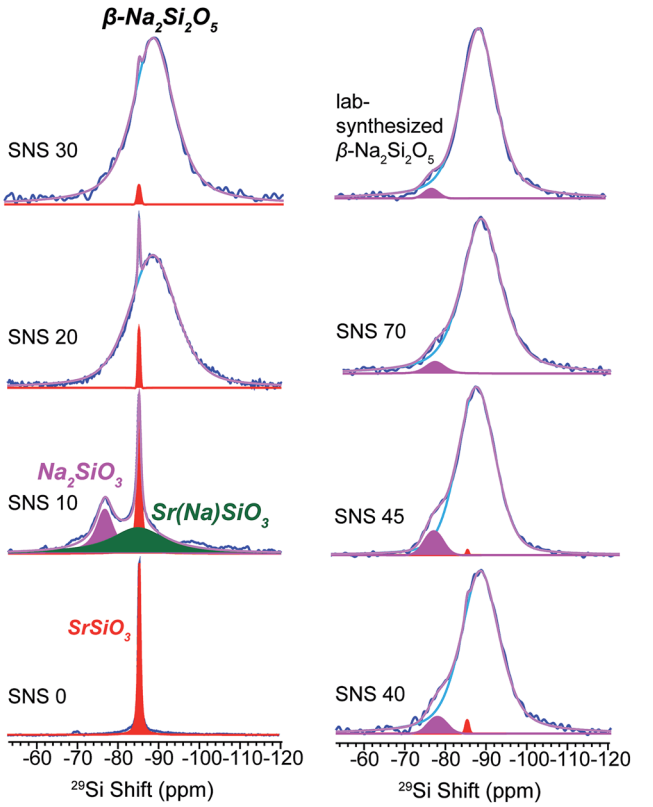

Fig. 1 ^{29}Si MAS NMR spectra of Na-doped $SrSiO_3$ (with apparent composition of $Na_xSr_{1-x}SiO_{3-0.5x}$) with different Na contents ($x = 0$, 0.1, 0.2, 0.3, 0.4, 0.45 and 0.70, denoted as SNS0, SNS10, SNS20, SNS30, SNS40, SNS45 and SNS70, respectively) and lab-synthesized β-$Na_2Si_2O_5$. Relevant resonance assignments, including $SrSiO_3$ (red), $SrSiO_3$ with Na doped within the structure (Sr(Na)SiO_3, green), Na_2SiO_3 (magenta), and β-$Na_2Si_2O_5$ (blue) are marked on the spectra. Spectral simulations are displayed together with the experimental spectra. All the NMR parameters used for the simulations are listed in Table S1.†

−85 ppm, assigned to Si_3O_9 sites in α-$SrSiO_3$.[4–7] With 10 mol% Na doping (SNS10), three distinct Si local environments are observed. In addition to the α-$SrSiO_3$ resonance at −85 ppm, a broad component centred also at −85 ppm and a third peak at −77 ppm are shown. The α-$SrSiO_3$ peak slightly broadens with the full width at half maximum (FWHM) increased from 40 Hz in SNS0 to 66 Hz in SNS10 compared with that of SNS0, suggesting long-range structural effects of Na doping. The broad resonance at −85 ppm with a FWHM of 0.93 kHz is from Si close to doped Na in the α-$SrSiO_3$ phase, *i.e.* Sr(Na)SiO_3 in Fig. 1, which accounts for about 1/3 of total Si amount. Significant difference in ^{29}Si T_1 relaxation times between the sharp (>10 s) and broad (<1 s) ^{29}Si moieties is observed. The −77 ppm peak is from the Q_2 site of Na_2SiO_3. This peak is also seen as a minor component with slight variation in percentage in other samples such as SNS40, SNS45, and synthesized β-$Na_2Si_2O_5$. Na_2SiO_3 is readily observed due to the similar conditions for synthesis as for SNS samples.[20]

As the Na doping content is further increased to more than 10 mol%, a broad ^{29}Si peak centred at −89 ppm gradually replaces the α-$SrSiO_3$ resonance (−85 ppm, sharp) and the

resonance of Si close to doped Na ($Sr(Na)SiO_3$, −85 ppm, broad). This new peak bears close resemblance to the ^{29}Si resonance of synthesized β-$Na_2Si_2O_5$, a broad peak centred at −89 ppm with a FWHM of 0.62 kHz (top right in Fig. 1). With Na content more than 40 mol%, very little change in the ^{29}Si spectra is observed, except slight narrowing of the −89 ppm peak. The original α-$SrSiO_3$ resonance is barely visible and the Na_2SiO_3 peak appears as a very minor component.

^{29}Si NMR is a good probe for changes in the SiO_x framework; however, it reveals very little information about the functional ions, *i.e.*, Na and O ions. ^{23}Na and ^{17}O NMR are more direct tools for studying the structure–function relationship in ion conductors but less commonly employed due to much greater challenges in data acquisition and analysis compared with NMR of spin-1/2 nuclei such as ^{29}Si. ^{23}Na and ^{17}O are both quadrupolar nuclei with non-integer spins ($I = 3/2$ for ^{23}Na and 5/2 for ^{17}O, respectively) and are thus subject to quadrupolar effects displacing resonances from their isotropic chemical positions. The strong quadrupolar interactions significantly broaden NMR spectra and thus compromise spectral resolution. Advanced capabilities, including fast sample spinning, high magnetic fields, and special techniques such as multiple-quantum MAS NMR, have been implemented to achieve high resolution. Spectral deconvolution combined with DFT NMR calculations helps to further resolve various Na and O local environments.

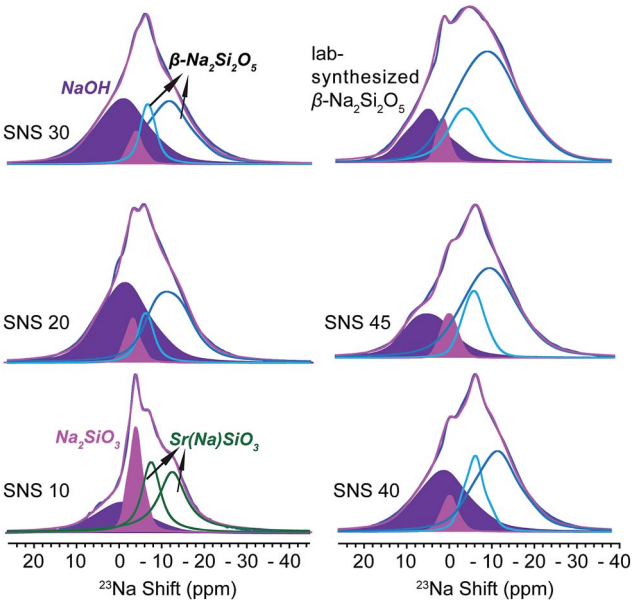

Fig. 2 ^{23}Na MAS NMR spectra of SNS10, SNS20, SNS30, SNS40, SNS45, and lab-synthesized β-$Na_2Si_2O_5$. Relevant resonance assignments, including $SrSiO_3$ with Na doped within the structure ($Sr(Na)SiO_3$, green), Na_2SiO_3 (magenta), NaOH (purple), and β-$Na_2Si_2O_5$ (cyan and blue) are marked on the spectra. Spectral simulations are displayed together with the experimental spectra. All the parameters used for the simulations are listed in Table S2.†

Fate of doped Na

^{23}Na NMR is helpful in identifying the local structural and compositional environments of the doped Na ions, which sheds light on the underlying reasons why Na doping improves the ionic conductivity of SNS.

As seen in Fig. 2, four Na resonances are observed in the ^{23}Na NMR spectra of all SNS samples. The two resonances at high field (small chemical shifts) in the ^{23}Na spectrum of SNS10 are from Na in the $SrSiO_3$ phase, *i.e.* $Sr(Na)SiO_3$. These two Na sites in $Sr(Na)SiO_3$ are quite different from those in β-$Na_2Si_2O_5$, which was found in SNS samples with higher Na contents. The C_Q (quadrupolar couplings constant, a measure of the strength of quadrupolar couplings) values of the two Na sites in $Sr(Na)SiO_3$ are 1.8 MHz and 0.47 MHz, respectively, while the typical C_Q values of the two Na sites in crystalline β-$Na_2Si_2O_5$ are 2.3 MHz.[20] In SNS samples with higher Na contents (>10 mol%), these two Na resonances convert to resonances similar to those of the synthesized β-$Na_2Si_2O_5$ (Fig. 2). The larger C_Q values (2.4 and 4.3 MHz) of ^{23}Na NMR resonances for the synthesized β-$Na_2Si_2O_5$ (2.3 MHz), compared with those for crystalline β-$Na_2Si_2O_5$, suggest significant structural disorder of the synthesized β-$Na_2Si_2O_5$. It is worth noting that the synthesized β-$Na_2Si_2O_5$ phase is not pure, which contains 4 mol% of crystalline Na_2SiO_3 and 15% NaOH. Again, it was reported previously that the synthesis condition for Na_2SiO_3 and β-$Na_2Si_2O_5$ are very similar and co-existence of these phases were observed.[20]

The remaining two peaks in the spectrum of SNS10 are from impurity phases, the broad peak at 8 ppm with a relatively large C_Q of 3.5 MHz is assigned to NaOH, based on the ^{23}Na NMR shift and C_Q of NaOH in previous reports.[21] This assignment is confirmed by comparing the ^{23}Na NMR spectra of NaOH, SNS30, and β-$Na_2Si_2O_5$ (see Fig. S1†). The peak next to the NaOH resonance is from Na_2SiO_3, of which the isotropic shift is −1.1 ppm and C_Q 2.0 MHz. Very little variations are observed for the resonances of NaOH and Na_2SiO_3 in SNS samples with increasing Na contents. The content of NaOH and Na_2SiO_3 remains below 10 mol% in SNS samples, and fluctuates (Table S5†) without a trend, likely depending on possible temperature variations during the synthesis and exposure to H_2O in the air.

Changes of O^{2-} environments

Since SNS was designed for use as an oxide ion conductor in intermediate-temperature SOFCs, the effects of Na doping on local structural environments and dynamics of oxide ions are most relevant for its intended applications. ^{17}O NMR is a powerful tool to probe the local environments and to investigate the dynamics of oxide ions. The extremely low sensitivity of ^{17}O NMR renders the data acquisition very challenging. In order to obtain ^{17}O NMR spectra with good signal-to-noise ratios for reliable interpretation, ^{17}O-isotope enrichment of SNS samples was carried out. The sensitivity of ^{17}O NMR was enhanced by a factor of around 180 times, which is equivalent to 0.037 mol% × 180 = 6.66 mol% ^{17}O in the isotope-enriched samples. The ^{17}O isotope enrichment was achieved through the isotope exchange of ^{16}O in the sample with ^{17}O in the $^{17}O_2$ gas, and the enrichment level strongly depends on the diffusivity of

oxide ions in the sample. This relatively low enrichment level (<10 mol%) suggests low O^{2-} diffusivity in SNS (Fig. S2†).

The enrichment process with careful temperature and time control does not alter the structure of pristine SNS samples, indicated by the resemblance of the ^{17}O spectra of SNS45 with and without isotope enrichment, shown in Fig. S2.† This resemblance also suggests non-preferential enrichment of different oxygen sites and implies that all oxide ions have equally low diffusivity.

^{17}O MAS NMR spectra of ^{17}O-enriched SNS10, SNS30 and SNS45 samples are shown in Fig. 3. In the ^{17}O spectrum of SNS10, the two resonances in red are assigned to α-$SrSiO_3$. Of the two resonances, the one with an isotropic shift of 109 ppm and a C_Q of 2.8 MHz is assigned to the non-bridging oxygen (nbo) sites in α-$SrSiO_3$ and the other with a chemical shift of 79 ppm and a C_Q of 3.9 MHz is from the bridging oxygen (bo) sites in α-$SrSiO_3$.[22] The ratio of the nbo to bo sites is very close to 2 : 1, consistent with the crystal structure of α-$SrSiO_3$. A very broad peak spanning over more than 250 ppm with a centre around 126 ppm is likely from the disordered O sites in the Sr(Na)SiO_3 phase. The great breadth of this ^{17}O NMR peak echoes with the large linewidth of the ^{29}Si NMR resonance of the same phase. This phase contains about 27% of the total oxygen content. The weak and broad resonance at 66 ppm with a C_Q around 8.3 MHz is assigned to NaOH. Naturally, the resonances of Na_2SiO_3 are seen, with the peak from the bo site at 72 ppm with a C_Q of 4.7 MHz and that of the nbo site at 39 ppm with a C_Q of 2.3 MHz. The ratio of these two oxygen sites is 1 : 1, which agrees with the structure of Na_2SiO_3. The oxygen fraction from the impurity phases, *i.e.*, NaOH and Na_2SiO_3 is less than 10 mol%.

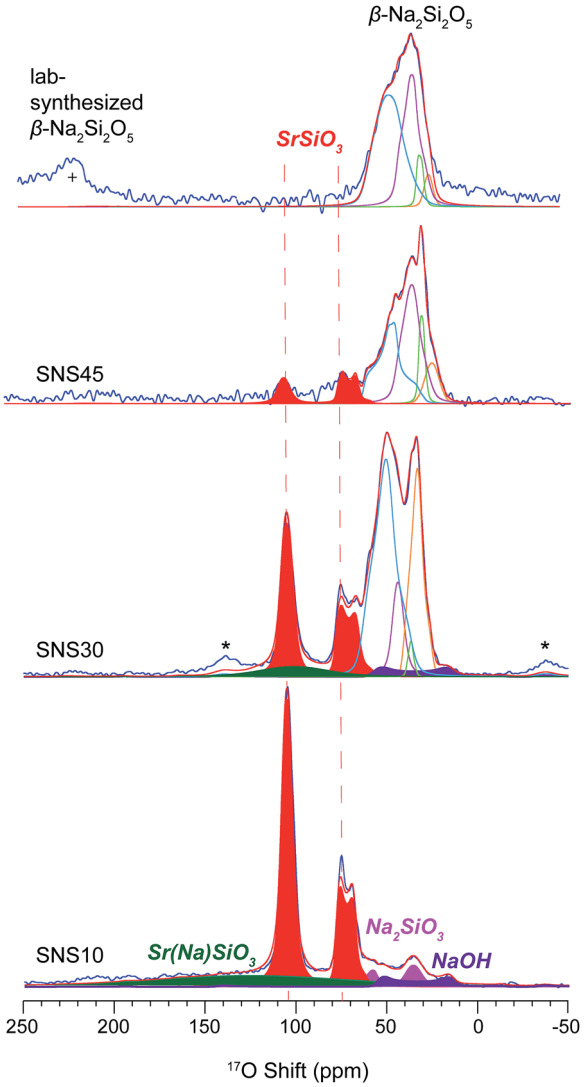

Fig. 3 ^{17}O MAS NMR spectra of SNS10, SNS30, SNS45, and lab-synthesized β-$Na_2Si_2O_5$. All the samples are ^{17}O-isotope enriched, except the synthesized β-$Na_2Si_2O_5$. Relevant resonance assignments, including $SrSiO_3$ (red), $SrSiO_3$ with Na doped within the structure (Sr(Na)SiO_3, green), Na_2SiO_3 (magenta), NaOH (purple), and β-$Na_2Si_2O_5$ (cyan and blue lines) are marked on the spectra. Spectral simulations (red lines) are displayed together with the experimental spectra (blue lines). All the parameters used for the simulations are listed in Table S3.† * marks the spinning sidebands. + denotes the one of the spinning sidebands from the ^{17}O NMR resonance of ZrO_2 rotor at 370 ppm.

In the ^{17}O spectrum of SNS30, the ^{17}O peaks at 109 ppm and 80 ppm are assigned to an intermediate Sr-rich phase transformed from α-$SrSiO_3$ due to Na doping, but with significant reduction in intensity compared with those of α-$SrSiO_3$ in SNS10. The content of the nbo sites is reduced from 40% to 15%, while that of the bo sites from 19% to 10%. The increase in the ratio of bo sites to nbo sites from 2 : 1 (in SNS10) to 3 : 2 (in SNS30) suggests fusion of the metasilicate structural framework. The weak broad Sr(Na)SiO_3 resonance is also observed with the position shifted to higher field by 25 ppm (from 126 ppm in SNS10 to 101 ppm in SNS30). Our DFT calculations also show ^{17}O resonances of O sites close to Na appearing at a higher field than those of O sites further away from Na (Fig. S4†) The content of Sr(Na)SiO_3 is decreased from 27% in SNS10 to 6% in SNS30. At the expense of Sr-rich phases, the percentage of the β-$Na_2Si_2O_5$-like phase grows, manifested by multiple resonances between 10–65 ppm. Four ^{17}O environments are resolved with spectral analysis based on typical C_Q and shifts from our DFT calculations and previous reports.[23] The 63 ppm resonance with a C_Q of 4.5 MHz is very similar to the ^{17}O NMR signature of one of the bo sites in β-$Na_2Si_2O_5$ (Fig. 3 and Table S3†). The other bo site (with a shift of 47 ppm and a C_Q of 2.7 MHz) has a smaller shift and C_Q compared with the corresponding site in β-$Na_2Si_2O_5$. The resonances with shifts of 40 and 39 ppm and C_Q values of 3.3 MHz and 2.1 MHz, respectively, are assigned to nbo sites of this β-$Na_2Si_2O_5$-like phase.

The ^{17}O spectrum of SNS45 is dominated by peaks primarily from the β-$Na_2Si_2O_5$ phase, accounting for about 88% of the total O content. The remaining O comes from the Sr-rich phase. The β-$Na_2Si_2O_5$ phase in SNS45 resembles very closely the synthesized β-$Na_2Si_2O_5$, suggested by similar ^{17}O resonances. The two resonances at lower field with shifts of 58 ppm and 41 ppm and C_Q values of 5.0 MHz and 4.0 MHz, respectively, are from the bo sites in β-$Na_2Si_2O_5$. The remaining two peaks with shifts of 30 ppm and 25 ppm and C_Q values of 2.1 MHz and 2.3 MHz, respectively, are from the nbo sites in β-$Na_2Si_2O_5$. The ^{17}O peaks in the spectrum of synthesized β-$Na_2Si_2O_5$ are slightly

broader than those of the β-$Na_2Si_2O_5$ phase in SNS45, indicating an increased degree in structural disorder.

The resonances from the Sr-rich phase at 109 ppm and 79 ppm are again reduced not only in peak intensity but also in the ratio of nbo-to-bo (from 3 : 2 in SNS30 to 1 : 1 in SNS45). The decrease in the ratio of nbo sites to bo sites indicates further fusion of the silicate framework. The ^{29}Si and ^{17}O signatures of this Sr-rich phase do not match those of Sr_2SiO_4 as proposed in previous report.[10]

Due to second-order quadrupolar broadening, the resolution of 1D ^{17}O NMR spectra is often insufficient for distinguishing individual oxide sites, despite that high magnetic field and fast MAS have been employed in the 1D ^{17}O NMR data acquisition. In order to achieve higher resolution, two-dimensional multiple quantum magic-angle spinning (MQMAS) NMR experiments were implemented to separate quadrupolar coupling effects from chemical shift interactions. Therefore, 1D ^{17}O projection NMR spectra with highest possible resolution could be obtained in the indirect dimension (F1 dimension or isotropic dimension). The quadrupolar pattern for each isotropic site can be extracted in the direct dimension (F2 dimension) for more accurate determination of quadrupolar parameters, which contains rich structural information.

The MQMAS NMR spectrum shown in Fig. 4 was acquired on ^{17}O-enriched SNS45. In the indirect (F1) dimension of the sheared 2D MQMAS NMR spectrum, a projection spectrum was obtained with six resonances shown at their isotropic shift positions. The corresponding quadrupolar pattern (Fig. 4a–f) for each resonance was extracted by taking a cross section along the F2 dimension at the respective isotropic shift position, which reveals information on the local environment of each oxygen site. The short ^{17}O T_2 relaxation times limit the resolution of the isotropic spectrum; therefore, overlap between the isotropic peaks in the F1 dimension is observed. As a result, the corresponding quadrupolar patterns are also overlapped to certain extent. Nevertheless, it is still possible to more clearly resolve individual O sites with MQMAS than with regular 1D ^{17}O MAS NMR. The isotropic shifts of the O sites are determined from the projection spectrum in F1 dimension and the corresponding quadrupolar coupling parameters are obtained from simulations of the cross sections in F2. Among the six components, the two at 28 ppm (Fig. 4a, red dashed line) and 32 ppm (Fig. 4b, green dashed line) are from the nbo sites in β-$Na_2Si_2O_5$; and the small quadrupolar couplings of 2.5 MHz and 2.8 MHz are close to our DFT calculations (Table S8†). Fig. 4d (navy blue dashed line), Fig. 4e (violet red and dodger blue lines), and Fig. 4f (dark red) show the quadrupolar patterns of the bo sites in β-$Na_2Si_2O_5$ with isotropic shifts at 45 ppm, 51 ppm and 58 ppm, respectively. Two of the three bo sites have similar C_Q (4.5 and 4.1 MHz) while the third site with the isotropic shift of 58

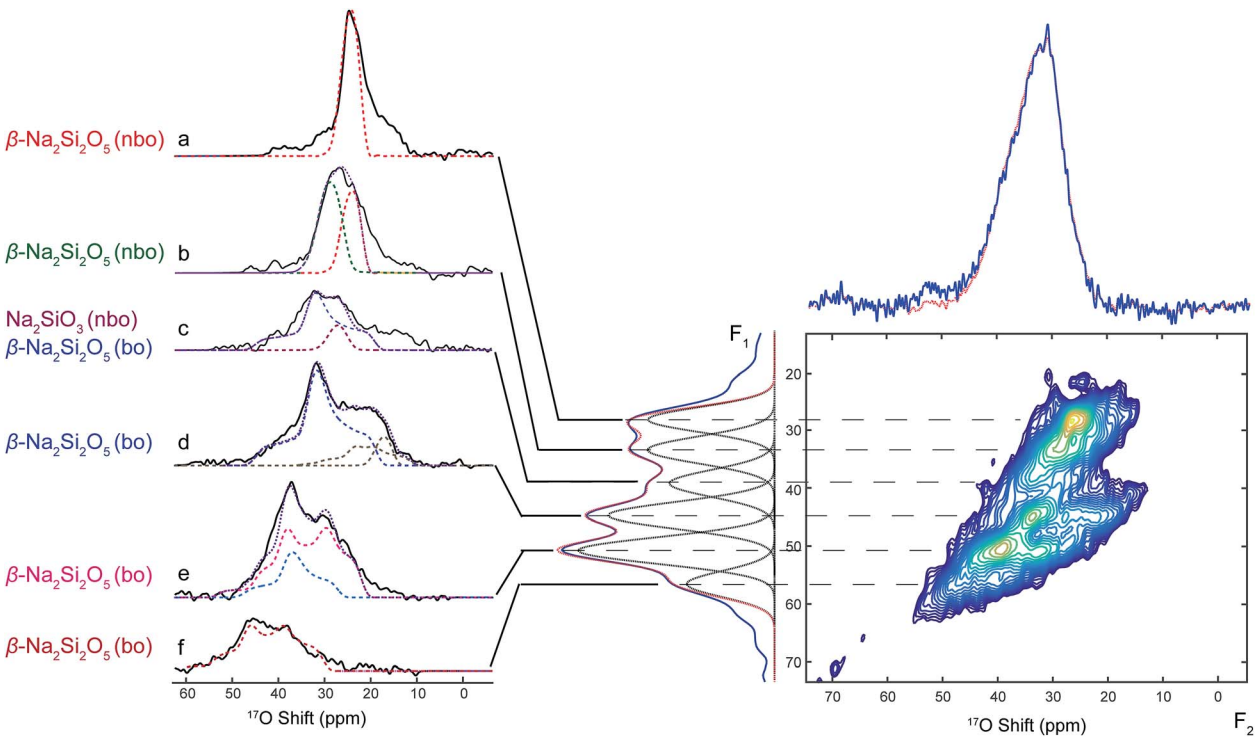

Fig. 4 ^{17}O multiple-quantum magic-angle spinning (MQMAS) NMR of ^{17}O isotope-enriched SNS45. The 1D quadrupolar patterns, labelled with (a)–(f), are cross sections from the 2D spectrum taken at the positions marked with dashed lines. Simulated patterns are overlapped with the cross sections. The purple dashed lines represent the sum of all simulated quadrupolar patterns for each spectrum in (a)–(f). The spectra on the top (red) and left (blue) of the 2D MQMAS spectrum are projections of the respective dimensions. The projection on the left (blue) is a sum of the isotropic spectra of various O sites and the simulated spectrum of each O site is also displayed (dotted lines under the projection spectrum). The projection (red) on the top of the 2D spectrum is overlapped with the regular MAS spectrum obtained at the same spinning speed as the MQMAS, *i.e.*, 10 kHz MAS.

ppm has a larger C_Q of 5.2 MHz. All the five oxygen sites in β-$Na_2Si_2O_5$ have been resolved with the MQMAS experiment and the results of spectral analysis assisted with simulations are consistent with our DFT NMR calculations (Table S8†).

Quantified evolution in SiO_x, Na, and O

Quantification of different chemical phases in SNS samples has been carried out based on the ^{29}Si, ^{23}Na, and ^{17}O NMR spectra. The results are summarized in Fig. 5, S4, and Tables S4–S6.† Although the accuracy of NMR quantification for quadrupolar nuclei is often compromised by different relaxation behaviours, it is still helpful to qualitatively follow the trend of phase evolution with increasing Na doping content in SNS. Quantification based on ^{29}Si, ^{23}Na, and ^{17}O NMR consistently indicates the same pattern of phase transition accompanied by structural transformation. The changes in the content of the three major phases, *i.e.*, α-$SrSiO_3$ (including $SrSiO_3$-derived phases), Sr(Na)SiO_3, and β-$Na_2Si_2O_5$, found in SNS upon increasing the Na doping content is illustrated in Fig. 5. It is shown that with little (<10 mol%) or no Na doping, α-$SrSiO_3$ is the dominant phase (> mol50%). As the Na doping amount is increased to 10 mol% (SNS10), the phase fraction of α-$SrSiO_3$ drops dramatically while the fraction of the intermediate phase Sr(Na)SiO_3 reaches its maximum. With further increase in Na-content to 20 mol%, α-$SrSiO_3$ continuously decreases to less than 10 mol%. Gradual conversion from the intermediate phase Sr(Na)SiO_3 to β-$Na_2Si_2O_5$ is observed. In SNS samples with more than 20 mol% Na doping, β-$Na_2Si_2O_5$ becomes the dominant component among the three major phases.

The complete quantification results, including impurity phases such as NaOH and Na_2SiO_3 and more detailed classification of various Na and O sites within the same phases, are documented in Tables S5 and S6 and plotted in Fig. S4.† A close examination of the evolution of various Na and O sites reveals information on gradual structure transition. Take the full quantification data from ^{23}Na NMR as an example first, the initial dose of Na goes into the pristine structure α-$SrSiO_3$ to form Sr(Na)SiO_3. The ratio of the two Na sites in Sr(Na)SiO_3 is 1 : 1. Further addition of Na leads to the formation of β-$Na_2Si_2O_5$ and the ratio of the two Na sites in β-$Na_2Si_2O_5$ stays nearly constant, *i.e.*, 1 : 3, similar to that in the lab-synthesized β-$Na_2Si_2O_5$. From the detailed quantification of ^{17}O NMR, we can also gain additional information regarding the structural changes. In the initial structure of α-$SrSiO_3$, the ratio of the nbo and bo is 2 : 1. The vanishing rates of these two O sites are quite different. The nbo sites disappearing much faster than the bo sites as Na is added into SNS, which brings the ratio of nbo and bo close to 1 : 1 in SNS45.

Na and O ion dynamics

The dynamics of Na^+ and O^{2-} have been probed *via* the changes in ^{23}Na and ^{17}O NMR spectral lineshape of SNS45 over a broad temperature range from room temperature (RT) to 618 °C. In ^{23}Na and ^{17}O MAS NMR, the spectral broadening is mainly due to the different orientations of crystallites in the powder sample, quadrupolar coupling, and dipolar coupling.[24] Ion motions at elevated temperatures average out some of the interactions and this motional effect manifests in the spectra as the narrowing of the peaks.

^{23}Na variable-temperature NMR spectra in Fig. 6a reveal gradual changes in Na^+ dynamics as the temperature is increased. At RT, a Gaussian lineshape is observed, broadened due to random crystallite orientations and ^{23}Na quadrupolar and dipolar couplings. As the temperature was increased to 419 °C, continuous narrowing of the peak occurs. Meanwhile, the transition from a Gaussian to a Lorentzian shape is seen. The linewidth of a solid-state NMR resonance is determined by homogeneous and/or inhomogeneous broadening. Inhomogeneous broadening is often resulted from a distribution of local structural environments of the nuclei and leads to a Gaussian lineshape. Homogeneous broadening is usually caused by the relaxation of the nuclear polarization. Ion dynamics modulates the local magnetic field and introduces perturbation to various spin–spin and spin–lattice interactions, and this perturbation

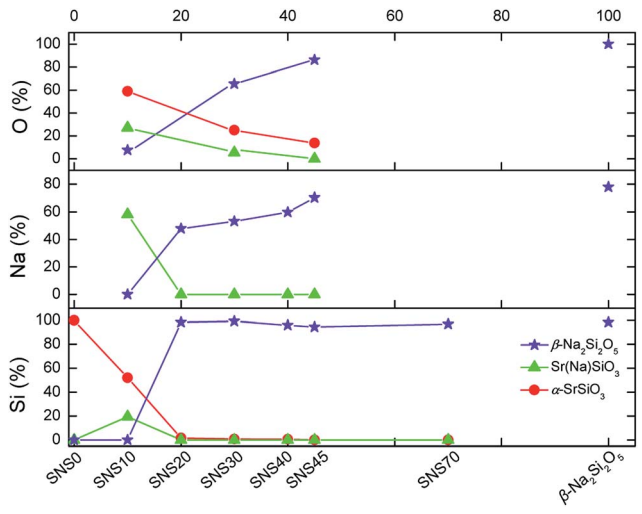

Fig. 5 Quantification of Si, Na, and O in various chemical phases in SNS samples based on the area integral of the ^{29}Si, ^{23}Na, and ^{17}O NMR spectra in Fig. 1–3.

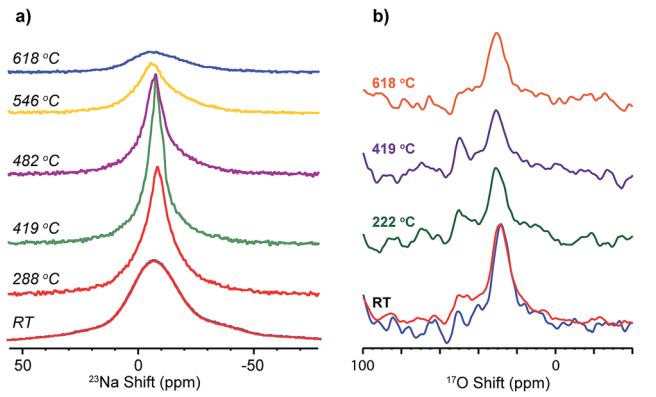

Fig. 6 Variable high-temperature (a) ^{23}Na, and (b) ^{17}O solid-state MAS NMR spectra of SNS45, acquired at a spinning speed of 5 kHz.

further manifests as exponential decay of the magnetization. The Fourier transform of an exponential decay yields Lorentzian lineshapes. More often than not, the lineshapes of NMR resonances are a combination of Gaussian and Lorentzian with one of them shown as the predominant feature. In the case of SNS, at low temperature, the Na ion dynamics is slow, and the relaxation of the magnetization is also relatively slow (as seen from T_1 relaxation time constant measurements of ^{23}Na NMR),[10] thus inhomogeneous broadening yields the observed Gaussian lineshape. The increase in temperature allows faster Na ion motions. On one hand, Na ion motion reduces inhomogeneous broadening by averaging out the orientation difference in local structural environments; on the other hand, faster Na ion motion leads to more rapid relaxation of ^{23}Na magnetization thus increased homogeneous broadening.[10] Therefore, diminishing inhomogeneous broadening and increasing homogeneous broadening give rise to a transition from a Gaussian to a Lorentzian lineshape of the ^{23}Na resonance at high temperatures. Further increase in temperature from 419 °C up to 618 °C returns ^{23}Na resonances back to a Gaussian shape with increased peak width. Upon slow cooling of the sample to RT, another spectrum was acquired, which overlays completely with the spectrum collected before variable-temperature experiments. ^{17}O NMR (Fig. 6b) shows little or no change in the peak shape or width as the temperature was increased from RT to 618 °C. The ^{17}O NMR spectra acquired before and after heating are very similar.

Discussion

Multinuclear high-resolution solid-state MAS NMR characterizations of the SNS series provide useful insights into the composition, structure, and ion dynamics of this fast ion conductor. ^{29}Si, ^{23}Na, and ^{17}O NMR have clearly and consistently revealed the gradual changes in chemical phase composition and structure with increasing Na doping amount. These gradual changes correlate well with the continuous improvement in ionic conductivity up to 45 mol% Na doping (SNS45).

With Na doping less than 10 mol% in SNS, the initial dose of Na incorporates into the α-$SrSiO_3$ structure to form a structurally disordered phase Sr(Na)SiO_3, *i.e.* $Na_xSr_{1-x}SiO_{3-0.5x}$. Approximately 46% of the original α-$SrSiO_3$ structure is affected by Na doping with 54% remaining crystalline. The disordered Sr(Na)SiO_3 and crystalline α-$SrSiO_3$ phases co-exist but are spatially separated. The spatial separation of Sr(Na)SiO_3 and α-$SrSiO_3$ is indicated by the significant difference in ^{29}Si T_1 relaxation times of Sr(Na)SiO_3 (<1 s) and α-$SrSiO_3$ (>10 s) resonances. This agrees with previous ToF-SIMS mapping of an analogous compound $Sr_{0.8}K_{0.2}Si_{0.5}Ge_{0.5}Si_{2.9}$ showing an inhomogeneous elemental distribution.[5] α-$SrSiO_3$ remains crystalline as shown by its sharp peak in ^{29}Si NMR and the two well-defined quadrupolar patterns in ^{17}O NMR. The area integral ratio of the two oxygen peaks representing the two oxygen sites (nbo and bo) in α-$SrSiO_3$ is 2 : 1, consistent with its crystal structure, which also supports that this phase remains largely unaffected by small amount of Na doping. In Sr(Na)SiO_3, strictly speaking, Na does not simply occupy the position of Sr; instead it takes up two inequivalent chemical sites. The local environments of these two Na sites, although bearing a certain degree of resemblance to the two Na sites in β-$Na_2Si_2O_5$, are better defined compared to those in β-$Na_2Si_2O_5$, as indicated by the relatively narrower linewidth. Also, the occupancy ratio of the two sites in Sr(Na)SiO_3 obtained from ^{23}Na NMR is close to 1 : 1, while in the synthesized β-$Na_2Si_2O_5$, the ratio of the two Na sites is found to be 1 : 3. Therefore, Sr(Na)SiO_3 is an intermediate phase from α-$SrSiO_3$ to β-$Na_2Si_2O_5$. The conductivity measurements of SNS showed that even with only 10 mol% Na doping, four orders of magnitude increase in ionic conductivity is observed compared with crystalline α-$SrSiO_3$.[7] Based on the analysis above, the source of the ionic conductivity boost is likely from the 46% disordered Sr(Na)SiO_3 phase with very little contribution from the 54% crystalline α-$SrSiO_3$ phase.

With Na doping content between 10–40 mol% in SNS, the crystalline α-$SrSiO_3$ phase continues to diminish and the remaining crystalline phase transforms to an intermediate Sr-rich phase, meanwhile a gradual phase transition from Sr(Na)SiO_3 to β-$Na_2Si_2O_5$ occurs. In this region, the α-$SrSiO_3$ phase decreases to less than 10% of its original quantity. Continuous fusion of the SiO_x framework in the Sr-rich phase is suggested by the increased ratio of bo to nbo sites in ^{17}O NMR. The Sr-rich phase still remains crystalline and isolated, as evidenced by the sharp resonance in ^{29}Si NMR and the well-defined quadrupolar ^{17}O NMR patterns. The β-$Na_2Si_2O_5$ phase grows at the expense of both α-$SrSiO_3$ and Sr(Na)SiO_3. The transition from Sr(Na)SiO_3 to β-$Na_2Si_2O_5$ is much faster than that from α-$SrSiO_3$ to Sr(Na)SiO_3. Therefore, Sr(Na)SiO_3 is hardly visible in SNS30 and beyond. As manifested in the gradual changes in the ^{23}Na and ^{17}O NMR resonances, the structural adjustment from Sr(Na)SiO_3 to β-$Na_2Si_2O_5$, occurs *via* a gradual instead of a one-step process. The shifts of the two Na peaks continuously move downfield close to those in β-$Na_2Si_2O_5$. Also, the ^{23}Na quadrupolar coupling constants are gradually increased to match those in β-$Na_2Si_2O_5$. The increase in quadrupolar coupling constants is a strong indication of structural disorder, which is promoted by the addition of Na into SNS. ^{17}O NMR data also clearly illustrates the progressive changes from a different perspective. ^{17}O NMR indicates that Sr(Na)SiO_3 first converts to a "β-$Na_2Si_2O_5$-like" phase with approximately equal amount of bo and nbo (terminal) sites while in the synthesized β-$Na_2Si_2O_5$ sample, there is much greater representation of bo than that of nbo; this indicates a re-adjustment of the SiO_x framework to facilitate the phase transition. The "β-$Na_2Si_2O_5$-like" phase has a more ordered structure compared with the synthesized β-$Na_2Si_2O_5$, as suggested by the relatively smaller ^{17}O C_Q parameters of the "β-$Na_2Si_2O_5$-like" resonances. In this region, the ionic conductivity continues to see significant improvement as the Na content is increased. This closely follows the trend of the continuous decrease in the content of the crystalline Sr-rich phase and increase in the fraction of structurally disordered component, *i.e.* the "β-$Na_2Si_2O_5$-like" phase.

With increasing Na content more than 40 mol% in SNS, a small decrease in the content and minimal structural changes of the Sr-rich phase are observed. Both ^{29}Si and ^{17}O NMR spectra suggest a Si_2O_5 network. In addition to the Sr-rich

phase, NMR signatures of the dominant phase formed in SNS are very similar as those of the synthesized β-$Na_2Si_2O_5$. The improvement in ionic conductivity beyond 40 mol% Na doping is very limited, which echoes with only small changes in composition or structure of the SNS composites.

Overall, Na doping into $SrSiO_3$ leads to formation of structurally disordered phases including Sr(Na)SiO_3 and β-$Na_2Si_2O_5$ and a crystalline Sr-rich phase. The content of Sr(Na)SiO_3 and β-$Na_2Si_2O_5$ correlates well with the change in the total ionic conductivity of SNS. No significant changes in structure or composition, thus ionic conductivity, have been observed for compositions with more than 40 mol% Na doping.

Na^+ and O^{2-} motions are probed by the variable high-temperature MAS NMR. The narrowing of ^{23}Na NMR peaks and the lineshape transformation from Gaussian to Lorentzian from RT to 419 °C indicate increase in Na^+ motions, consistent with a most recent ^{23}Na variable-temperature study over a range from room temperature to 350 °C.[10] Then with the temperature increased beyond 480 °C, the ^{23}Na peaks are broadened again accompanied by the return of a Gaussian lineshape. This unusual behaviour, deviating from expected further increase in Na ion motions with higher temperature, is likely caused by the onset of a crystallization process at high temperatures, which inevitably slows down the Na^+ ion motions. This is consistent with the recent degradation studies of amorphous $Na_2Si_2O_5$ at temperatures higher than 500 °C, which shows the transformation of amorphous $Na_2Si_2O_5$ to crystalline $Na_2Si_2O_5$ based on the high-temperature XRD data and decreased ionic conductivity was observed as a result of the phase transition.[8] On the other hand, no motional narrowing of the ^{17}O resonance was observed with temperature increased up to 618 °C, suggesting minimal O^{2-} motion. Based on the analysis above, it is likely that mainly Na ions are responsible for the high ionic conductivity measured at temperatures below 500 °C. This finding contradicts the earlier studies suggesting O^{2-} conduction in this material,[1,2] but agrees with recent reports showing that the material is virtually a mixture of amorphous $Na_2Si_2O_5$ and crystalline $SrSiO_3$;[5–8] the former has been predicted as a Na^+ conductor by MD simulations[9] and NMR measurements.[10]

It is worth noting that sufficient ion dynamics is a necessary condition for good ion conduction. Ion dynamics include both local motion and long-range diffusional motion, and only the diffusional motion effectively contributes to ion conduction. The ion diffusivity can often be measured by pulse field gradient (PFG) NMR. However, due to very short relaxation times on the order of milliseconds of ^{23}Na NMR resonance for SNS,[10] the estimated diffusivity based on the measured ion conductivity[1,2] is below the limit of the state-of-the-art PFG NMR for reliable detection (please refer to ESI† for detailed explanation).

Conclusion

The changes in structure, phase composition, and ion dynamics of a fast-ion conductor SNS with varying Na content have been probed with advanced solid-state NMR techniques. Detailed data analyses reveal that initial Na addition to the crystalline α-$SrSiO_3$ phase leads to the formation of a structurally disordered intermediate phase Sr(Na)SiO_3 and further increase in Na content promotes the gradual transformation of Sr(Na)SiO_3 to a "β-$Na_2Si_2O_5$-like" phase accompanied by fusion of the SiO_x network in the Sr-rich phase. Eventually β-$Na_2Si_2O_5$ appears as the dominant phase in SNS samples with >40 mol% Na doping. The decrease in the content of crystalline α-$SrSiO_3$ and increase in that of Sr(Na)SiO_3 and β-$Na_2Si_2O_5$ contribute to the significantly increased ionic conductivity in SNS. Variable-temperature ^{23}Na and ^{17}O NMR experiments reveal increased Na^+ motion but little O^{2-} motion as the temperature was increased from RT to 480 °C. Above ~480 °C, the Na^+ motion slows down likely due to early-stage crystallization, consistent with ionic conductivity measurements. Therefore, Na ions have been identified as the major charge carriers and are responsible for the observed high ionic conductivity of this material. The insights gained from careful investigations of the local structural environments and dynamics of potential charge carriers in SNS help clearly resolve the long-standing debate regarding the origin of high ionic conductivity observed in SNS. This study identifies SNS as a Na^+ conductor instead of an O^{2-} conductor, which means its application in intermediate-temperature SOFCs may not be suitable. It also confirms that the majority of doped Na does not replace Sr in the structure, but rather it resides in an amorphous β-$Na_2Si_2O_5$ phase. This research demonstrates that high-resolution high-temperature NMR can be a very powerful tool in addressing critical questions such as phase transition and ion transport in ion conductors.

Experimental section

Materials

SNS samples with $x = 0$, 0.1, 0.2, 0.3, 0.4, 0.45 and 0.7 in the apparent composition $Na_xSr_{1-x}SiO_{3-0.5x}$ were synthesized following the procedure detailed in previous studies,[1,2] and denoted as SNS0, SNS10, SNS30, SNS40, SNS45 and SNS70, respectively. β-$Na_2Si_2O_5$ was also made and used as a model material for phase identification in this study. The starting materials Na_2CO_3 (99.9%, Fisher Scientific, USA) and SiO_2 (99.9%, Alfa Aesar, USA) in the respective molar ratio of 1 : 2 were first mixed in a high-energy mechanical mixer (8000M Mixer/Mill®, SPEX® SamplePrep, USA) in the presence of ethanol. The dried mixture was pelletized at 5 MPa and calcined at 800 °C for 10 h. The pre-calcined pellets were then broken into fine particles of 1–2 μm in diameter with a high-energy vibrational mill (Micronizing Mill, McCrone, USA). After pelletizing again at a pressure of 75 MPa, the sample was eventually sintered at 900 °C for 10 h and gradually cooled down to room temperature with a rate of 2 °C min^{-1}.

The ^{17}O-enrichment of SNS samples was carried out by heating the SNS powder in a closed quartz tube filled with $^{17}O_2$ gas atmosphere (70%, Cambridge Isotope Laboratories) at 600 °C for 24 h followed by gradually cooling down to room temperature.

Solid-state NMR characterization

^{29}Si NMR spectra were acquired on a Bruker DRX-300 spectrometer at a Larmor frequency of 59.6 MHz using a Bruker

4 mm MAS probe spinning at 10 kHz. A rotor-synchronized spin-echo pulse sequence was employed. The 90° pulse length was 4.5 μs and the recycle delay was 2 s. A recycle delay of 100 s was also used when the crystalline phase $SrSiO_3$ is present to ensure accurate quantification. The ^{29}Si NMR shift of 4,4-dimethyl-4-silapentane-1-sulfonic acid at 0 ppm was used as the chemical shift reference.

To minimize broadening effects of quadrupolar couplings and to gain high resolution and sensitivity, ^{23}Na and ^{17}O NMR spectra were acquired on a Bruker DRX-830 spectrometer with a home-built 3.2 mm low-E and high-sensitivity MAS probe.[25] The Larmor frequency for ^{23}Na is 219.6 MHz and for ^{17}O is 112.6 MHz.

All ^{23}Na NMR measurements were carried out with a rotor-synchronized spin–echo pulse sequence at a MAS rate of 18 kHz. For the series of SNS samples and β-$Na_2Si_2O_5$, the solid 90° pulse length was 1.5 μs and the recycle delay was 0.5 s. All the ^{23}Na shifts were referenced to that of a 1 M NaCl solution at 0 ppm.

^{17}O MAS NMR experiments were carried out using the home-built 3.2 mm MAS probe spinning at a frequency of 18 kHz. A rotor-synchronized spin–echo pulse sequence was applied to ^{17}O-enriched SNS samples (SNS10, SNS30, and SNS45) and lab-synthesized β-$Na_2Si_2O_5$. The solid 90° pulse length was 2 μs and the recycle delay was 10 s. All of the ^{17}O shifts were referenced to H_2O(l) (0 ppm). The MQMAS spectrum of ^{17}O-enriched SNS45 was collected using a shifted-echo sequence using a home-built 4 mm single channel probe with a spinning speed of 10 kHz.[26] All r.f. pulse lengths were optimized on the SNS45 sample. The recycle delay was 1 s and a total of 51 200 scans were acquired for each of the 12 rotor-synchronized t_1 increments.

Variable high-temperature ^{23}Na and ^{17}O MAS NMR experiments were carried out with a rotor-synchronized spin-echo pulse sequence at a MAS speed of 5 kHz, using a Bruker 7 mm laser-absorption MAS probe on a Bruker Avance-600 spectrometer. Recycle delays of 1 s for both ^{23}Na and ^{17}O were used. Temperature was calibrated based on the temperature dependence of the ^{79}Br chemical shift of KBr.[27]

The spectral analyses and simulations of all 1D spectra were performed using the Topspin (v 3.2) software. MQMAS spectral processing and simulations were carried out with a MATLAB (v 8.5.1) script.

Acknowledgements

Y.-Y. Hu and P.-H. Chien acknowledge support from the National Science Foundation under Grant No. 1508404. K. Huang and Y. Lee acknowledge the Advanced Research Projects Agency-Energy (ARPA-E), U.S. Department of Energy for support under Award number DE-AR0000492.

Notes and references

1 P. Singh and J. B. Goodenough, *J. Am. Chem. Soc.*, 2013, **135**, 10149.
2 T. Wei, P. Singh, Y. Gong, J. B. Goodenough, Y. Huang and K. Huang, *Energy Environ. Sci.*, 2014, **7**, 1680.
3 R. Martinez-Coronado, P. Singh, J. Alonso-Alonso and J. B. Goodenough, *J. Mater. Chem. A*, 2014, **2**, 4355.
4 J. Xu, X. Wang, H. Fu, C. M. Brown, X. Jing, F. Liao, F. Lu, X. Li, X. Kuang and M. Wu, *Inorg. Chem.*, 2014, **53**, 6962.
5 R. D. Bayliss, S. N. Cook, S. Fearn, J. A. Kilner, C. Greaves and S. J. Skinner, *Energy Environ. Sci.*, 2014, **7**, 2999.
6 C. Tealdi, L. Malavasi, I. Uda, C. Ferrara, V. Berbenni and P. Mustarelli, *Chem. Commun.*, 2014, **50**, 14732.
7 I. R. Evans, J. S. O. Evans, H. G. Davies, A. R. Haworth and M. L. Tate, *Chem. Mater.*, 2014, **26**, 5187.
8 Y. Jee, X. Zhao and K. Huang, *Chem. Commun.*, 2015, **51**, 9640.
9 X. Lei, Y. Jee and K. Huang, *J. Mater. Chem. A*, 2015, **3**, 19920.
10 J. R. Peet, C. M. Widdifield, D. C. Apperley, P. Hodgkinson, M. R. Johnson and I. R. Evans, *Chem. Commun.*, 2015, **51**, 17163.
11 R. D. Bayliss, S. N. Cook, D. O. Scanlon, S. Fearn, J. Cabana, C. Greaves, J. A. Kilner and S. J. Skinner, *J. Mater. Chem. A*, 2014, **2**, 17919.
12 F. Blanc, D. S. Middlemiss, Z. Gan and C. P. Grey, *J. Am. Chem. Soc.*, 2011, **133**, 17662.
13 F. Blanc, M. Leskes and C. P. Grey, *Acc. Chem. Res.*, 2013, **46**, 1952.
14 R. Dervişoğlu, D. S. Middlemiss, F. Blanc, L. A. Holmes, Y.-L. Lee, D. Morgan and C. P. Grey, *Phys. Chem. Chem. Phys.*, 2014, **16**, 2597.
15 M. T. Dunstan, F. Blanc, M. Avdeev, G. J. McIntyre, C. P. Grey and C. D. Ling, *Chem. Mater.*, 2013, **25**, 3154.
16 Y. Yamazaki, F. Blanc, Y. Okuyama, L. Buannic, J. C. Lucio-Vega, C. P. Grey and S. M. Haile, *Nat. Mater.*, 2013, **12**, 647.
17 G. Kim, F. Blanc, Y.-Y. Hu and C. P. Grey, *J. Phys. Chem. C*, 2013, **117**, 6504.
18 L. Buannic, F. Blanc, D. S. Middlemiss and C. P. Grey, *J. Am. Chem. Soc.*, 2012, **134**, 14483.
19 R. Dervişoğlu, D. S. Middlemiss, F. Blanc, Y.-L. Lee, D. Morgan and C. P. Grey, *Chem. Mater.*, 2015, **27**, 3861.
20 X. Xue and J. F. Stebbins, *Phys. Chem. Miner.*, 1993, **20**, 297.
21 S. F. Dec, G. E. Maciel and J. J. Fitzgerald, *J. Am. Chem. Soc.*, 1990, **112**, 9069.
22 H. K. C. Timken, S. E. Schramm, R. J. Kirkpatrick and E. Oldfield, *J. Phys. Chem.*, 1987, **91**, 1054.
23 T. Charpentier, S. Ispas, M. Profeta, F. Mauri and C. J. Pickard, *J. Phys. Chem. B*, 2004, **108**, 4147.
24 A. M. George, P. Richet and J. F. Stebbins, *Am. Mineral.*, 1998, **83**, 1277.
25 (*a*) P. L. Por'kov, W. Mao, J. A. Kitchen, Z. Gan, J. Trebosc, J. P. Amoureux and W. W. Brey, *Presented at the 54th Experimental NMR Conference*, Pacific Grove, CA, April, 2013; (*b*) Z. Gan, P. L. Gor'kov, W. W. Brey, P. J. Sideris and C. P. Grey, *J. Magn. Reson.*, 2009, **200**, 2.
26 (*a*) A. Medek, J. S. Harwood and L. Frydman, *J. Am. Chem. Soc.*, 1995, **117**, 12779; (*b*) Z. Gan and H.-T. Kwak, *J. Magn. Reson.*, 2004, **168**, 346.
27 K. R. Thurber and R. Tycko, *J. Magn. Reson.*, 2009, **196**, 84.